ACS OMEGA

http://pubs.acs.org/journal/acsodf

Article

# Gold and Platinum Nanoparticle-Functionalized $TiO_2$ Nanotubes for Photoelectrochemical Glucose Sensing

Zhuo Yang, Wei Xu, Bingdong Yan, Baiqiang Wu, Jinxin Ma, Xiaohong Wang, Bin Qiao, Jinchun Tu, Hua Pei, Delun Chen,* and Qiang Wu*

Cite This: *ACS Omega* 2022, 7, 2474−2483

Read Online

ACCESS | Metrics & More | Article Recommendations | Supporting Information

**ABSTRACT:** Developing stable photoelectrochemistry (PEC) glucose biosensors with high sensitivity and a low detection limit is highly desirable in the biosensor field. Herein, a highly sensitive and stable enzymatic glucose PEC biosensor is rationally designed and fabricated using a $TiO_2$NTs/Au/Pt/GOx electrode. First, we prepared one-dimensional $TiO_2$ nanotube arrays which could realize the orthogonalization of the light-incident direction and the carrier diffusion direction via anodization. Subsequently, we used the method of photoassisted deposition for anchoring Pt nanoparticles on $TiO_2$NTs after electrodepositing Au nanoparticles. Among them, Au nanoparticles promote light absorption via the surface plasmon resonance effect and the separation of photogenerated carriers through forming a Schottky junction. Moreover, the Pt nanoparticles on the electrode surface can react with hydrogen peroxide ($H_2O_2$) generated from glucose (Glu) oxidation by glucose oxidase (GOx), accelerating the electron-transfer process during glucose oxidation and greatly improving the sensitivity of the glucose biosensor. As a result, $TiO_2$NTs/Au/Pt/GOx exhibited excellent PEC performance, achieving a high sensitivity of 81.93 $\mu$A $mM^{-1}$ $cm^{-2}$ and a low detection limit (1.39 $\mu$M), far exceeding the performance of $TiO_2$NTs/M/GOx (M = Au, Pt). Therefore, the introduction of Pt nanoparticles as active substances to promote enzymatic reactions is important for designing high-performance enzyme biosensors.

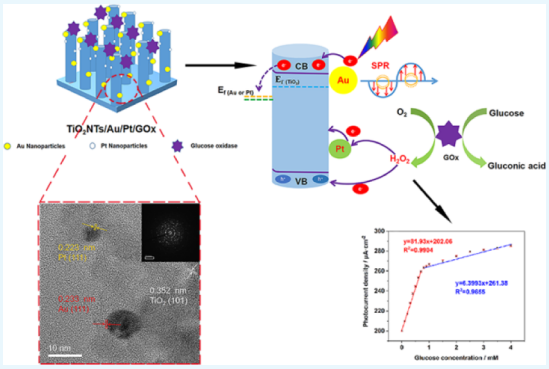


## 1. INTRODUCTION

Biosensor research has focused on the development of a simple sensing technology with fast detection, high sensitivity, and low interference.[1] The photoelectrochemistry (PEC) process consists of a photoelectric conversion (the main process) and an electrochemical process, which produces a highly sensitive and accurate signal with low background signal noise through the interaction of the optical and electrochemical systems.[2] In addition, PEC-based enzyme biosensors can solve the problem of poor selectivity in traditional bioanalysis techniques.[3] Therefore, the photoactive material not only acts as an energy converter to generate photogenerated carriers upon irradiation but also provides a site for the target receptors in PEC to selectively identify and capture the target analyte.[4]

Titanium dioxide is a common semiconductor material, which has been widely used in various photoelectrocatalytic processes for its strong oxidizing capacity and photostability. According to the unique photoelectric properties of titanium oxide, researchers have developed advanced optoelectronic materials for high-performance PEC biosensing through forming heterojunctions,[5] introduction of wide band gap semiconductors,[6] and defect engineering[7] methods. The regular arrangement of $TiO_2$ nanotubes ($TiO_2$NTs), which has proven to be a good photoanode material,[8] prepared by anodic oxidation can be used for the photolysis of water,[9] in purification,[10] as an antibacterial,[11] and for photovoltaic power generation.[12] However, the rapid recombination of photocarriers and the narrow light absorption range severely limit the performance of PEC and their applications. It has been proposed to extend the lifetime of photocarriers by controlling charge transfer to achieve an enhanced PEC performance.[13] Noble metals can be introduced to augment the rate of electron transfer. Melvin et al. supported the Au−Pt alloy on the surface of $TiO_2$ and used the bimetal as an electron absorber to enhance the photocatalytic performance.[14] They found that Au and Pt supported on $TiO_2$ can be used as electron absorbers to weaken the rapid recombination of carriers. Wu et al. have reported that the modification of Au nanoparticles on the surface of $TiO_2$NTs can produce the surface plasmon resonance (SPR) effect, increase the absorption of ultraviolet−visible light, and enhance the

**Received:** December 1, 2021
**Accepted:** December 29, 2021
**Published:** January 6, 2022

Scheme 1. Manufacturing Process of the $TiO_2$NTs/Au/Pt/GOx Biosensor

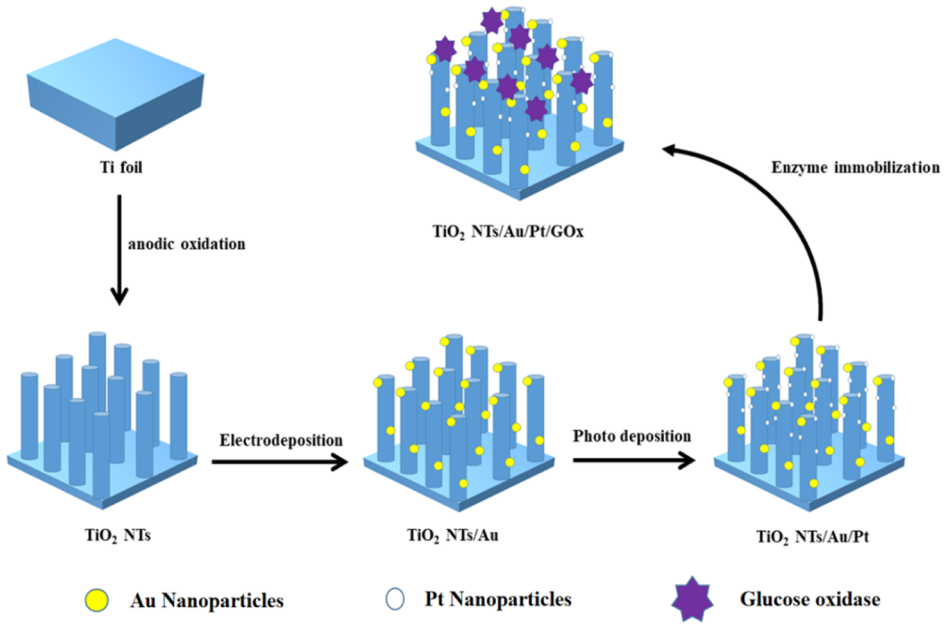


photocatalytic activity.[15] In the above studies, the application of Pt mainly improved the performance of PEC by changing the charge behavior of the material. Few people have mentioned the strategy of improving the sensitivity of the PEC enzymatic glucose biosensor by catalytically decomposing $H_2O_2$ during the enzymatic reaction of platinum nanoparticles. In the present study, we constructed a bimetal (Au, Pt) nanoparticle-loaded $TiO_2$NTs/Au/Pt/GOx biosensor for glucose detection.

In this study, ultrahigh sensitivity of the $TiO_2$NTs/Au/Pt/GOx biosensor was obtained by the following design concepts. Au nanoparticles are loaded to increase the conductivity and improve the narrow light absorption range of the material and the serious problems of electron−hole recombination.[16] At the same time, Pt nanoparticles are deposited, and Pt is used as an important active substance to catalyze the decomposition of $H_2O_2$ under the enzymatic reaction,[17] resulting in the accelerated consumption of hydrogen peroxide and the transfer of electrons in the enzymatic reaction, thereby achieving ultrahigh sensitivity for the PEC enzymatic glucose biosensor.

## 2. RESULTS AND DISCUSSION

The synthesis process diagram of the PEC biosensor is exhibited in Scheme 1. The Ti foil was etched to prepare $TiO_2$NTs. Subsequently, Au and Pt nanoparticles were deposited on the $TiO_2$ film through electrochemical and light deposition, respectively. Next, glucose oxidase and chitosan were dropped evenly on the electrode surface.

Based on the scanning electron microscopy (SEM) image in Figure 1a, the prepared $TiO_2$ nanotube film shows a vertical one-dimensional tubular shape. In Figure 1b, the diameter and thickness of the nanotube are 80 and 20 nm, respectively. As shown in Figure S1, because of the lower loading of Au and Pt nanoparticles, no considerable change was observed on the electrode surface before and after introducing precious metals compared with other electrodes. The high-resolution transmission electron microscopy (HR-TEM) image of $TiO_2$NTs deposited with Au and Pt is shown in Figure 1d. Figure 1c,d shows a large amount of Au and PtNPs with a size range of 6−12 nm attached to $TiO_2$ nanotubes. The edge of the $TiO_2$NTs/Au/Pt (Figure 1d) lattice fringe is 0.352 nm. The (101) crystal plane of $TiO_2$ corresponds to anatase. Lattice fringes of 0.223 and 0.233 nm are identified as the (111) crystal plane of Pt and Au, respectively. Figure 1e−i shows the high-angle annular dark-field−scanning transmission electron microscopy (HAADF-STEM) and element mapping results, in which Ti, O, Au, and Pt are uniformly distributed, confirming that Au and Pt NPs are homogeneously loaded on $TiO_2$NTs. Figure 1j shows the EDS energy spectrum of $TiO_2$NTs/Au/Pt. The content of noble metals is less, especially Pt. This also leads to the failure to show the 4f peak of Pt in the subsequent XPS test.

Based on XRD tests on the electrodes, we analyzed the material structure of the electrode material. As shown in Figure 2a, the peak of the Ti foil is indexed to the JCPDS database (44-1294), and the peaks located on 25.28, 37.8, and 48.05° are assigned to the (101), (004), and (200) crystal facets of anatase titanium dioxide (JCPDS 21-1272), respectively. Moreover, after loading precious metal NPs on the $TiO_2$ film, the XRD peaks of $TiO_2$ did not change. This indicates that the crystal structure of titanium dioxide has not changed to form an alloy after loading precious metals. At the same time, because the precious metals are highly dispersed and the particle size is small, their XRD peaks are not detected.

To further investigate the electronic interactions of $TiO_2$ with Au and Pt, we carried out the XPS test. Figure 2b shows that the peaks located at 458.9 and 464.6 eV represent Ti 2p 3/2 and 1/2, respectively, indicating that only tetravalent titanium ions for $TiO_2$ nanotubes are present. Meanwhile, the signals of Au 4f 7/2 and Au 4f 5/2 at 83.4 and 87.1 eV, respectively, are the characteristic peaks of Au (in Figure 2c), while its 83.7 eV spin energy separation is consistent with the published results on the spin energy separation of Au NPs.[18] In addition, the poor S/N ratio reflects the lower content of AuNPs deposited on the surface of $TiO_2$ nanotubes, accounting for only 3.6% of the content. Moreover, compared with the characteristic peak of the standard Au,[18] the apparent negative shift of Au 4f indicates that the Au surface is in an


https://doi.org/10.1021/acsomega.1c06787
ACS Omega 2022, 7, 2474−2483

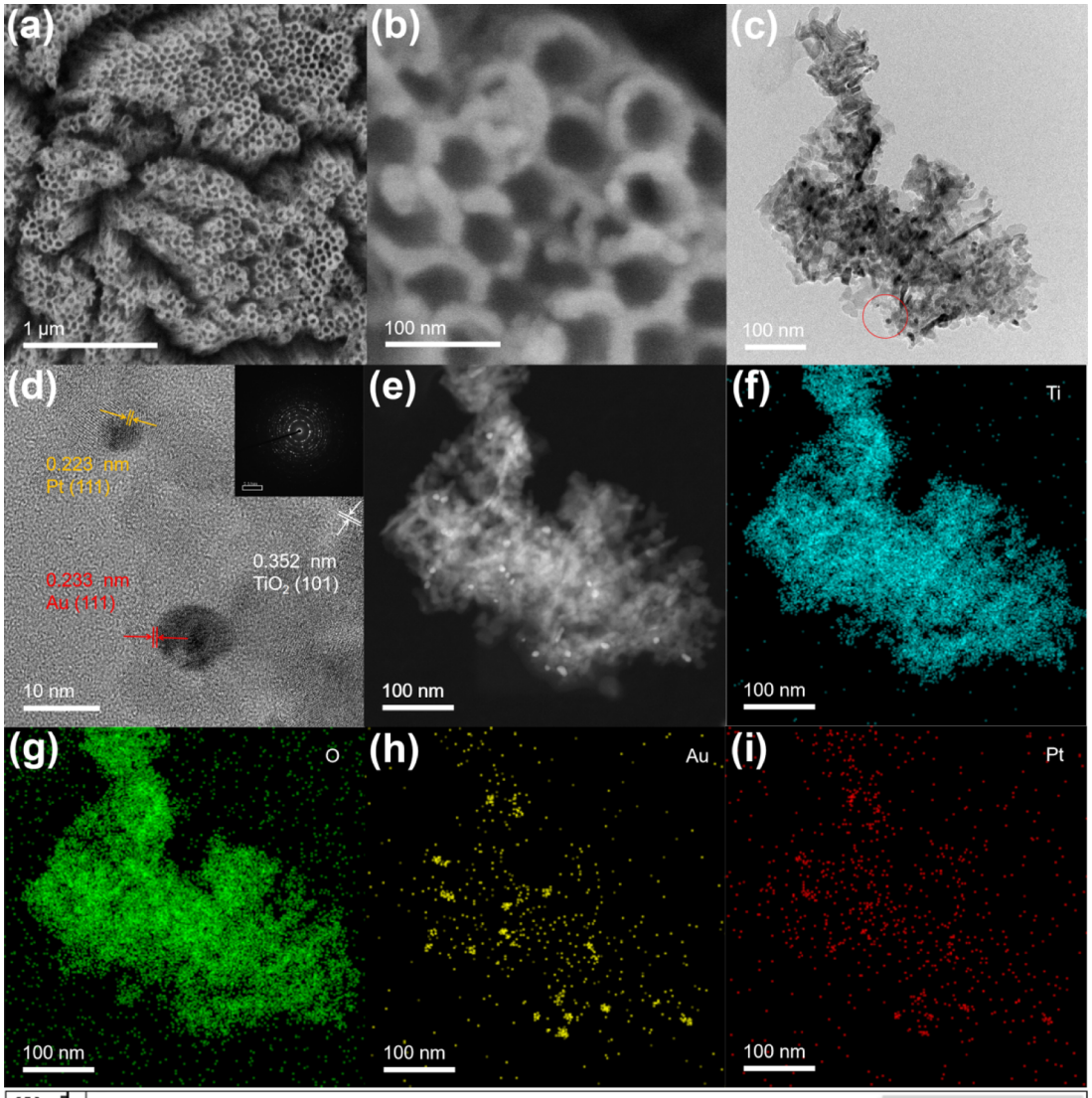


| Element | Wt% | Wt% Sigma |
|---|---|---|
| O | 40.93 | 0.30 |
| Ti | 55.18 | 0.31 |
| Pt | 0.30 | 0.17 |
| Au | 3.60 | 0.22 |
| Total: | 100.00 | |

**Figure 1.** b) SEM images of $TiO_2$NTs/Au/Pt; (c,d) TEM and HR-TEM images of $TiO_2$NTs/Au/Pt; (e–i) HAADF-STEM and mapping of Ti, O, Au, and Pt of $TiO_2$NTs/Au/Pt; and (j) EDS spectra of $TiO_2$NTs/Au/Pt.



https://doi.org/10.1021/acsomega.1c06787
ACS Omega 2022, 7, 2474−2483

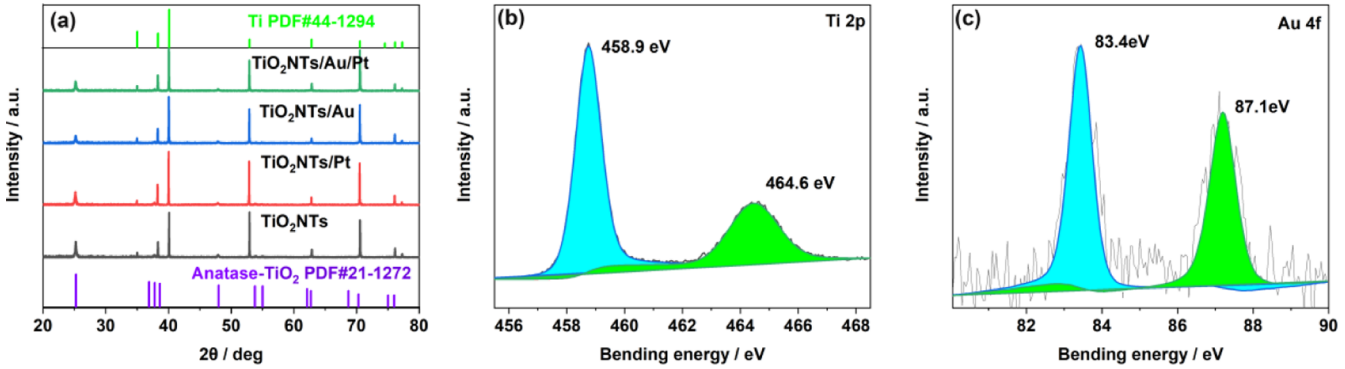


**Figure 2.** (a) XRD patterns of $TiO_2$NTs, $TiO_2$NTs/Pt, $TiO_2$NTs/Au, and $TiO_2$NTs/Au/Pt; (b) XPS spectra for Ti 2p; and (c) Au 4f core level for $TiO_2$NTs/Au/Pt.

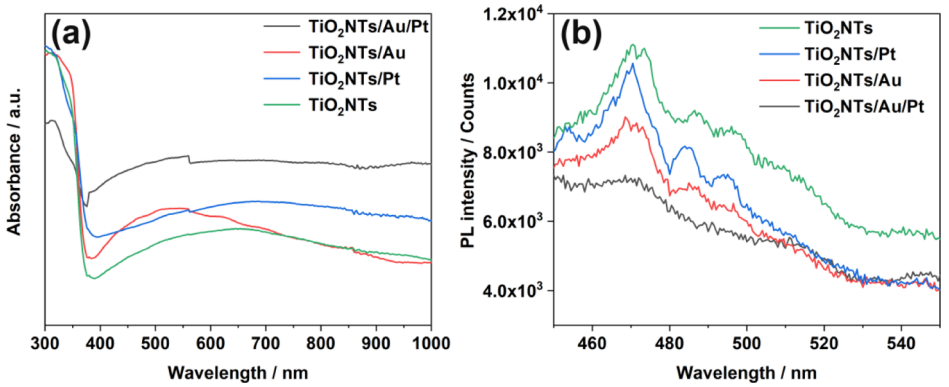


**Figure 3.** (a) UV−vis absorption spectra and (b) PL spectra of $TiO_2$NTs, $TiO_2$NTs/Pt, $TiO_2$NTs/Au, and $TiO_2$NTs/Au/Pt in the powder form at 350 nm excitation.

electron-rich state. This suggests that in the contact between metallic Au and $TiO_2$, considering that the Fermi energy levels of Au and $TiO_2$ are different, the energy level difference can be balanced through the migration of electrons from the surface of $TiO_2$ to Au, causing part of the metal−semiconductor contact to bend the Fermi surface and form a Schottky junction. Similar results were reported by Melvin et al.,[14] in which a low amount of Pt with a relatively scattered distribution was loaded on the sample surface, and the signal of Pt 4f was not found by XPS detection.

UV−visible absorption spectra were measured for all four systems ($TiO_2$NTs, $TiO_2$NTs/Pt, $TiO_2$NTs/Au, and $TiO_2$NTs/Au/Pt) and are shown in Figure 3a. All four photoelectrodes show an obvious absorption cutoff edge near the anatase maximum absorption wavelength of 387 nm. This finding confirms that the load of the noble metal does not change the inherent absorption of $TiO_2$. Moreover, considering that the bimetal does not have light absorption in the characteristic absorption range of titanium dioxide, after the bimetal was loaded, the absorption peak near the characteristic absorption wavelength of titanium dioxide decreased. In comparison with the curve of titanium dioxide, $TiO_2$NTs/Au exhibited a strong visible light absorption near 550 nm, which is attributed to the SPR absorption of AuNPs.[19] Therefore, gold could act as an effective light collector in terms of the characteristics of UV−vis plasma (collective and strong oscillation of delocalized conduction electrons)[20] and enhance the photoelectric catalytic activity of the material.

The photoluminescence spectrum (PL) was obtained to further study the four different materials. At an excitation wavelength of 350 nm, a series of emission characteristic peaks were obtained for the material appearing between 400 and 500 nm. Based on Figure 3b, the emission intensities were obtained and can be arranged as $TiO_2$NTs > $TiO_2$NTs/Pt > $TiO_2$NTs/Au > $TiO_2$NTs/Au/Pt. The pure $TiO_2$NTs have high PL intensity, indicating the serious recombination of photogenerated electrons and holes. Considering that the level of emission intensity determines the degree of photogenerated electron−hole pair compounding, PL tests have demonstrated that the formation of a Schottky junction can store a certain number of electrons, thus effectively separating electron−hole pairs and avoiding charge compounding. The bimetallic-loaded electrode greatly reduced the PL intensity compared with the electrode loaded with noble metal nanoparticles alone, suggesting that the loading of Au and Pt NPs resulted in a synthetic effect. Therefore, the recombination of electron holes was greatly reduced.

The electrochemical and PEC experiments were carried out to examine the PEC performance of the $TiO_2$NTs, $TiO_2$NTs/Pt, $TiO_2$NTs/Au, and $TiO_2$NTs/Au/Pt electrodes. In Figure 4a, the results of PEC show that the values of photocurrent density are in the following order: $TiO_2$NTs/Au/Pt > $TiO_2$NTs/Au > $TiO_2$NTs/Pt > $TiO_2$NTs. The results confirmed that precious metals are beneficial for the photovoltaic performance. The SPR effect of Au can increase the light absorption of $TiO_2$, thus intensifying the photocatalytic activity of the material. Second, the loading of Au and Pt can form a Schottky junction on the surface of $TiO_2$NTs and promote the separation of photocarriers, thereby improving the photocurrent response. However, considering that a few



https://doi.org/10.1021/acsomega.1c06787
ACS Omega 2022, 7, 2474−2483

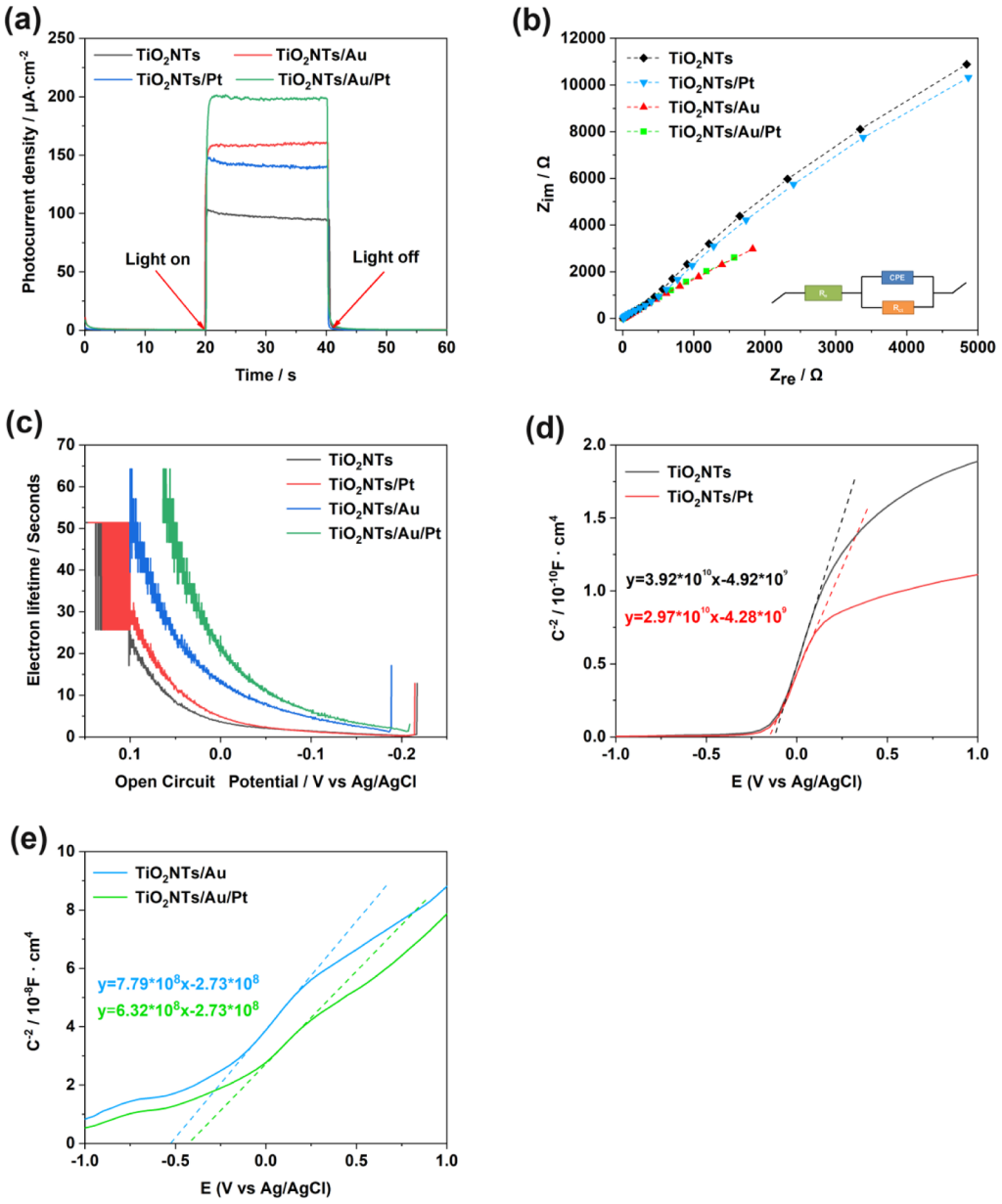


**Figure 4.** (a) Photoelectric response of $TiO_2$NTs, $TiO_2$NTs/Pt, $TiO_2$NTs/Au, and $TiO_2$NTs/Au/Pt under simulated sunlight (bias voltage = 0.4 V, 0.1 M PBS, pH = 7.4); (b) electrochemical impedance spectra of Nyquist plots; (c) electronic lifetime measurement determined from the decay of the open-circuit potential in the absence of light; and (d,e) Mott−Schottky plot in the dark at a fixed frequency of 5 kHz.

PtNPs are present on the electrode, the findings were not proved in XPS. However, Guo et al. found that the Schottky junction can be formed by loading Pt on the surface of $TiO_2$, thus promoting the photocatalytic activity.[21] This finding confirms why Pt can synergistically reduce the electron−hole recombination rate in the PL test.

As is known, electrochemical impedance spectroscopy (EIS) is one of the most commonly used methods to study the characteristics of the photoelectrode interface. The equivalent circuit (the inset in Figure 4b) is used for the Nyquist plots recorded from different samples. Among them, Re represents the system resistance, CPE represents the capacitance phase of the interface between the electrolyte and the photoelectrode, and Rct represents the transfer resistance of the charge carriers on the interface. The Nyquist plots of the $TiO_2$NTs/Au/Pt electrode in Figure 4b show the smallest arc diameter, indicating the lowest charge-transfer resistance and the fastest electron migration rate for this electrode.[22]

Figure 4c shows the open-circuit photovoltage decay (OCPVD) experiments, which were executed to further investigate the electronic behavior and to estimate the electronic lifetime generated under light according to the following equation[23]

$$\tau = \frac{k_B T}{e}\left(\frac{dV_{OC}}{dt}\right)^{-1}$$

In this equation, $\tau$ indicates the photoelectron lifetime, $k_B$ represents the Boltzmann constant, $T$ is the temperature, $V_{OC}$ represents the open-circuit voltage at the corresponding time, and $e$ represents the charge of an individual electron. As shown in Figure 4c, the electrode $TiO_2$NTs/Au/Pt has the longest carrier lifetime, which contributes to its PEC performance. In


https://doi.org/10.1021/acsomega.1c06787
ACS Omega 2022, 7, 2474−2483

addition, to determine its carrier density ($N_D$), we performed electric capacity analysis on the electrode/electrolyte with the following equation[24]

$$\frac{1}{C^2} = \frac{2}{N_D e \varepsilon_0 \varepsilon}\left[(U_S - U_{FB}) - \frac{k_B T}{e}\right]$$

In this equation, $C$ represents the space charge capacitance in the semiconductor interface, $N_D$ represents the density of carriers in the semiconductor, $e$ refers to the charge of a single electron, $\varepsilon_0$ represents the vacuum dielectric constant, $\varepsilon$ represents the relative dielectric constant of the semiconductor, $U_S$ is the applied potential, $T$ represents the temperature, and $k_B$ represents the Boltzmann constant. $N_D$ is determined from the MS plots as $1/C^2$ versus potential in Figure 4d,e by using the following equation[24]

$$N_D = -\left(\frac{2}{e\varepsilon\varepsilon_0}\right)\left(\frac{d\left(\frac{1}{C^2}\right)}{d(U_S)}\right)^{-1}$$

Finally, we obtained the following carrier concentration relationship: $TiO_2$NTs < $TiO_2$NTs/Pt < $TiO_2$NTs/Au < $TiO_2$NTs/Au/Pt. The significant increase of $N_D$ and $\tau$ confirms the deposition of Au and Pt NPs by forming Schottky junctions, thereby decreasing the recombination of photogenerated electrons with holes and increasing carrier concentration. Hence, the carrier lifetime improved PEC performance.

To demonstrate that Pt has a catalytic effect for $H_2O_2$, during the testing of glucose sensitivity, we performed cyclic voltammetry (CV) tests under light-free conditions. As shown in Figure S3a,b, the current density of $TiO_2$NTs and $TiO_2$NTs/Au electrodes without PtNPs were only elevated by 2 and 2.7 $\mu$A cm$^{-2}$ at 0.4 V (vs Ag/AgCl), respectively, when we added 1 mM hydrogen peroxide to the buffer. The current was enhanced probably caused by the electrolytic reaction of hydrogen peroxide. However, considering that Pt could decompose hydrogen peroxide in the solution and generate a number of electrical signals under the applied potential of the catalytic oxidation, the current densities between the $TiO_2$NTs/Pt and $TiO_2$NTs/Au/Pt electrodes modified with PtNPs differed with values of 12.7 and 13 $\mu$A cm$^{-2}$ at 0.4 V (vs Ag/AgCl), respectively (Figures S3c, 5). Therefore, PtNPs can catalyze hydrogen peroxide to enhance electron transfer in enzymatic reactions.

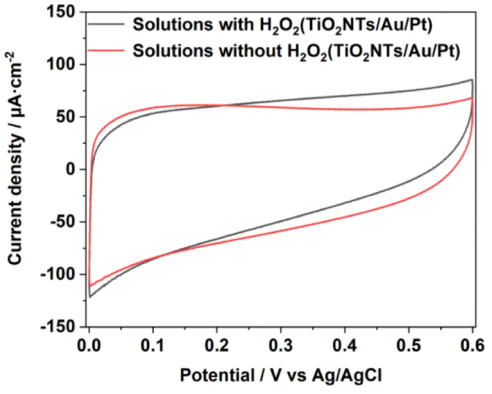


**Figure 5.** CV comparison in 0.1 M pH = 7.4 PBS solution with and without a $H_2O_2$ chart of $TiO_2$NTs/Au/Pt.

Generally, the capability of a biosensor is evaluated in terms of its sensitivity, limit of detection (3S/N), and linear range. As shown in Figure 6a, the photoelectric response of the $TiO_2$NTs/Au/Pt/GOx electrode was tested at stepped glucose concentrations under continual churning, and the photocurrent increased with increasing glucose concentration, indicating the sensitive response of the electrode to Glu concentration. Based on Figure 6b, the linear regression equation between glucose concentration and photocurrent is shown, where $j = 81.93x + 202.06$ at glucose concentrations between 0 and 0.8 mM and $j = 6.39x + 261.38$ when the glucose concentration is in the range of 0.8−4 mM. Thus, at glucose concentrations of 0−0.8 mM, the sensitivity was 81.93 $\mu$A mM$^{-1}$ cm$^{-2}$, and the LOD was 1.39 $\mu$M. At glucose concentrations of 0.8−4 mM, the sensitivity was 6.39 $\mu$A mM$^{-1}$ cm$^{-2}$. The segmentation of the test results is mainly attributed to the adsorption of intermediates by the electrode. At lower concentrations of glucose, the linearity shows a good relationship with a higher slope as a result of the free pervasion of glucose molecules toward the electrode at lower concentrations. At higher concentrations, the interaction between the glucose molecules intensifies, resulting in a less linear curve with a lower slope. Accordingly, two different sensitivities are observed at different linear ranges.[25]

To stress the advantages of $TiO_2$NTs/Au/Pt/GOx biosensors more intuitively, we conducted the same condition test on $TiO_2$NTs/Au/GOx, $TiO_2$NTs/Pt/GOx, and $TiO_2$NTs/GOx. The test results at the same concentration are shown in Figure S2. The sensitivity of the $TiO_2$NTs/GOx biosensor without Au and Pt NPs is only 8.53 $\mu$A mM$^{-1}$ cm$^{-2}$, and the linear range is 0−1 mM. Besides, the detection limit increased to 61.1 $\mu$M. The $TiO_2$NTs/Pt/GOx biosensor loaded with Pt has a sensitivity of 20.9 $\mu$A mM$^{-1}$ cm$^{-2}$, a linear range of 0−1 mM, and a detection limit of only 3.07 $\mu$M. The $TiO_2$NTs/Au/GOx biosensor loaded with Au only has a sensitivity of 39.58 $\mu$A mM$^{-1}$ cm$^{-2}$, a linear range of 0−0.7 mM, and a detection limit of 13.5 $\mu$M. In the linear range of 0−0.8 mM, the $TiO_2$NTs/Au/Pt/GOx biosensor had the highest sensitivity and the lowest LOD. This finding was observed because the SPR effect of Au enhanced light absorption, which is conducive to the generation of more photogenerated holes. In addition, the Au and Pt NPs synergistically promoted the valid separation of photogenerated electron−hole pairs through the formation of Schottky junctions between the metal and the semiconductor. The number of photogenerated holes in the material is dominant for the improvement of sensitivity. Therefore, the increase of photogenerated holes and the decrease of electron−hole recombination can improve the sensitivity to glucose. Moreover, the sensitivity of the PEC enzymatic biosensor was improved by the enhanced electron transfer in the enzymatic reaction catalyzed by the loaded PtNPs with hydrogen peroxide. Notably, the linear range of $TiO_2$NTs/Au/Pt/GOx at low sensitivity increased by 0.1 mM compared with $TiO_2$ NTs/Au/GOx, precisely because the catalytic effect of Pt accelerates the consumption of hydrogen peroxide on the electrode surface and reduces the molecular interactions, thus increasing the linear detection range of the electrode at low sensitivity.

Furthermore, we demonstrated the stability of the biosensor on the $TiO_2$NTs/Au/Pt/GOx electrode by switching $i$−$t$ response by 10 times. Figure 6c shows that the photocurrent response increased rapidly and remained stable for a few seconds after the light was switched on, while the magnitude of


https://doi.org/10.1021/acsomega.1c06787
ACS Omega 2022, 7, 2474−2483

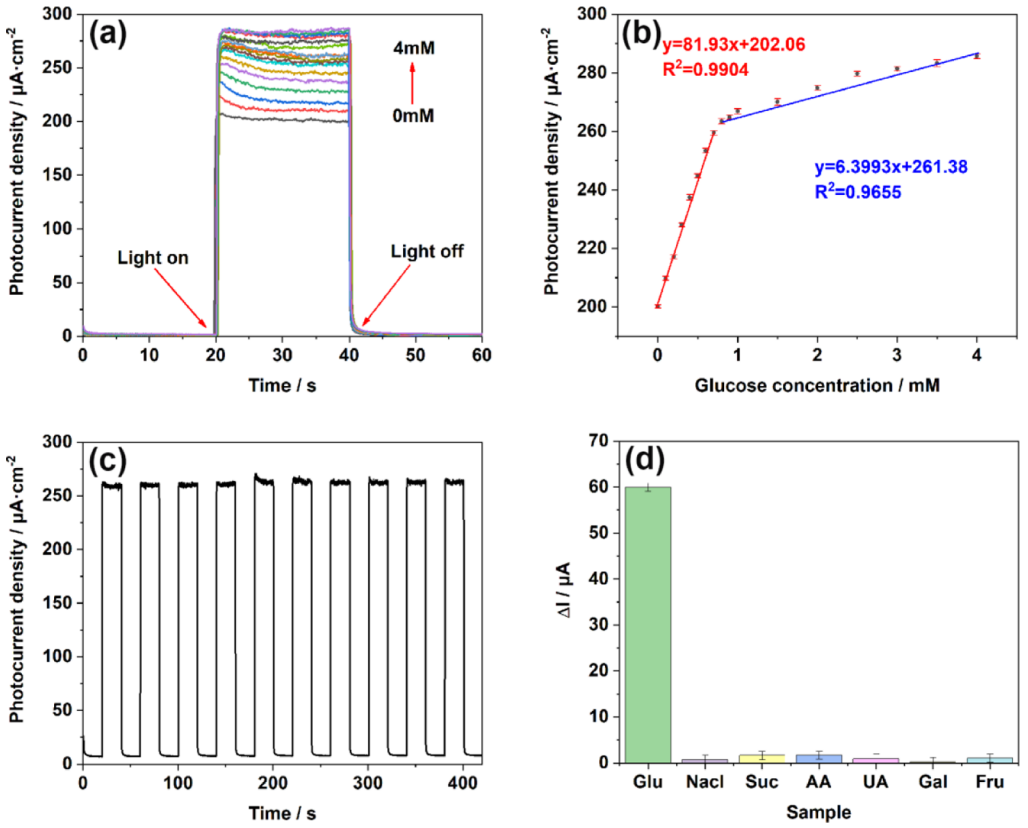


**Figure 6.** (a) *i*–*t* responses of $TiO_2$NTs/Au/Pt toward Glu at concentrations of 0–4 mM in the supporting electrolyte of 0.1 M PBS (pH = 7.4); (b) linear calibration curve (glucose concentration vs photocurrent density); (c) stability after addition of 1 mM glucose under light conditions; and (d) anti-interference performance test performed in 0.1 M PBS (pH = 7.4) at concentrations of 0.1 mM chloride (NaCl), sucrose (Suc), ascorbic acid (AA), uric acid (UA), galactose (Gal), and fructose (Fru).

**Table 1. Comparison of the Analytical Performance of PEC Glucose Biosensors**

| PEC biosensors | dynamic range (mM) | LOD ($\mu$M) | sensitivity ($\mu$A mM$^{-1}$ cm$^{-2}$) | ref |
|---|---|---|---|---|
| $TiO_2$-CNT-$Co_3O_4$ | 0–4 | 0.16 | 0.3 | 26 |
| FTO/$Fe_2O_3$-NB-PDA-GDH | 0–2 | 25.2 | 7.36 | 27 |
| Nafion/GOx/Ag-Pdop@CNT/GCE | 0.05–1.1 | 17 | 3.1 | 28 |
| GOx/TCS-$TiO_2$/chitosan/GCE | 0.005–1.32 | 2 | 23.2 | 29 |
| $TiO_2$ NTs/GOx | 0–1, 1–4 | 61.1 | 8.53, 2.98 | this work |
| $TiO_2$ NTs/Pt/GOx | 0–1, 1–4 | 3.07 | 20.9, 5.40 | this work |
| $TiO_2$ NTs/Au/GOx | 0–0.7, 0.7–4 | 13.5 | 41.73, 4.73 | this work |
| $TiO_2$ NTs/Au/Pt/GOx | 0–0.8, 0.8–4 | 1.39 | 81.93, 6.39 | this work |

the photocurrent remained stable after 10 repeated switches, with negligible changes in the photocurrent at each period.

Considering that the molecular interferents such as sodium chloride (NaCl), sucrose (Suc), ascorbic acid (AA), uric acid (UA), galactose (Gal), and fructose (Fru) normally coexist in human serum, we investigated their effects at certain concentrations of the biosensing response of the electrodes.

As shown in Figure 6d, the PEC test was performed under the same conditions of detecting, and the selectivity of the $TiO_2$NTs/Au/Pt/GOx electrode was investigated based on the photocurrent response plots after the addition of different interferents (0.1 mM). By comparing the biosensing response of the interferer with that of glucose to the electrode, almost no change was observed in photocurrent after the addition of the interferer. Hence, the $TiO_2$NTs/Au/Pt/GOx biosensor maintained its high selectivity for glucose.

As shown in Table 1, the $TiO_2$NTs/Au/Pt/GOx biosensor has higher sensitivity and better detection limits than the other PEC glucose biosensors.

We tried to explain the mechanism for PEC detection of glucose at enzyme modification electrodes as shown in Scheme 2. The modification of the electrode by Au and Pt NPs has an important effect on the PEC generation of photogenerated electrons and holes on the external of $TiO_2$. The SPR effect of AuNPs enhanced the absorption of light; meanwhile, high-energy charge carriers are generated during the plasma decay process,[30] thereby improving the catalytic activity of the electrode. Moreover, Au and Pt NPs can form a Schottky junction with $TiO_2$, which could reduce the recombination of photogenerated electrons and holes and increase the carrier lifetime. After loading GOx, glucose was present in the PBS electrolyte solution, glucose oxidase gradually oxidized glucose into gluconic acid and $H_2O_2$ (formula 1), and the holes in the $TiO_2$NTs/Au/Pt/GOx electrode could capture the enzymatic


https://doi.org/10.1021/acsomega.1c06787
ACS Omega 2022, 7, 2474–2483

**Scheme 2. Mechanism of Action of the $TiO_2$NTs/Au/Pt/GOx PEC Biosensor for Glucose Detection**

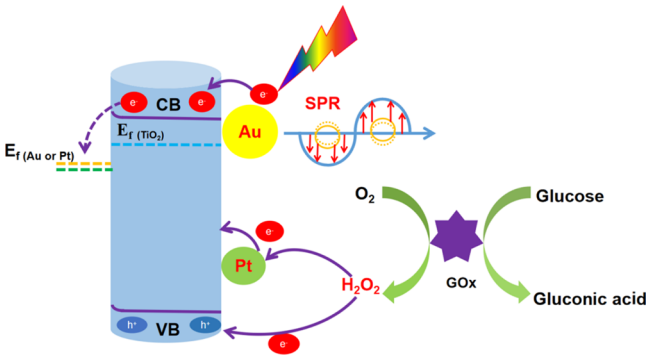


products for redox reactions and generate a photocurrent (formula 3, photoelectrocatalytic reaction). Besides, the PtNPs loaded on the surface of $TiO_2$ promoted the decomposition of hydrogen peroxide because of their strong catalytic activity, which enhanced the transfer of electrons in the enzymatic reaction and further enhanced the current response to glucose (formula 4, electrocatalytic reaction). Therefore, when the glucose concentration was varied, different electrical signals were generated. The reaction formula is as follows

$$\text{glucose} + O_2 \xrightarrow{\text{GOx}} \text{gluconic acid} + H_2O_2 \quad (1)$$

$$h\nu \rightarrow h^+ + e^- \quad (2)$$

$$H_2O_2 + h^+ \rightarrow H_2O + H^+ \quad (3)$$

$$H_2O_2 - e^- \xrightarrow{\text{Pt}} O_2 + H^+ \quad (4)$$

## 3. CONCLUSIONS

In summary, we have successfully designed the high-performance PEC biosensor for glucose testing based on $TiO_2$NTs/Au/Pt nanocomposites. Gold nanoparticles enhanced the conductivity of the electrode and promoted the absorption of light via the SPR effect and the separation of photogenerated carriers in the material through forming a Schottky junction. Subsequently, the catalytic activity of the electrode was greatly improved. At the same time, PtNPs can catalyze the decomposition of $H_2O_2$ in the enzymatic reaction to enhance the transfer of electrons in the enzymatic reaction and further enhance the PEC performance of the sensor. Finally, the obtained $TiO_2$NTs/Au/Pt/GOx PEC biosensor has good stability and selectivity in the linear range of 0−0.8 mM and from 0.8 to 4 mM, where the sensitivities are 81.93 and 6.39 $\mu A\ mM^{-1}\ cm^{-2}$, and the detection limit is low at 1.39 $\mu$M. Inspired by demonstrating the excellent performance of the $TiO_2$NTs/Au/Pt/GOx PEC biosensor for glucose detection performance, the introduction of active substances will promote the process of enzymatic reactions, possibly resulting in the quick transfer of electrons in enzymatic reactions to further improve the performance of the sensor, which will be a new approach for building other high-performance PEC enzymatic biosensors.

## 4. EXPERIMENTAL SECTION

**4.1. Fabrication of $TiO_2$NTs.** Before the anodizing treatment, the pretreated titanium foil sample (10 × 20 × 0.25 mm) was polished for 30 s and then washed in acetone, ethanol, and deionized water for 5 min by ultrasonication and dried in air at 50 °C. Afterward, anodic oxidation was performed in an electrochemical cell with titanium foil as the working electrode and a stainless-steel sheet as the counter electrode. The electrolyte consists of a glycol system containing 0.5 wt % ammonium fluoride and 6 vol % deionized water. Under magnetic stirring with a direct current power supply, anodization was carried out for 30 min under a 60 V bias. Then, the sample was sonicated with deionized water for 30 min (smooth surface) and anodized again for 90 min under a bias of 20 V. Subsequently, it was cleaned twice with ethanol ultrasonically and dried naturally. Finally, the specimen obtained by anodization was placed in a crucible and annealed at 400 °C in air for 3 h with a heating rate of 2 °C/min.

**4.2. Deposition of AuNPs on the $TiO_2$NT Photoelectrode.** Chloroauric acid was used as the precursor, Ag/AgCl was used as the reference electrode, and the Pt sheet was used as the counter electrode. Gold nanoparticles were electrochemically deposited in 0.1 M phosphate buffer (PBS, pH = 7.4). The traditional three-electrode system adopts the CV method, and the voltage range is from −1.25 to −0.7 V (reverse) with different cycles (0, 5, 10, 15 and 20 cycles). Afterward, the prepared $TiO_2$NTs/Au was washed with deionized water and dried in a vacuum oven at 70 °C for 12 h.

**4.3. Deposition of PtNPs onto the $TiO_2$NTs/Au Photoelectrode.** Platinum nanoparticles were loaded on $TiO_2$NTs by UV lamp deposition. Chloroplatinic acid was added to 30 mL of deionized water containing 10 mL of methanol. Then, the prepared $TiO_2$NTs/Au electrode was placed in the above solution and irradiated with a UV lamp for 0, 5, 10, 15, and 20 min. Subsequently, the prepared $TiO_2$NTs/Au/Pt was washed with deionized water several times and dried in a vacuum oven at 70 °C for 12 h.

**4.4. Deposition of GOx onto the $TiO_2$NTs/Au/Pt Photoelectrode.** Glucose oxidase is loaded on the target electrode by the drop coating method. Glucose oxidase was first coated on the electrode surface and kept at 4 °C for 24 h. Subsequently, chitosan solution dissolved in acetic acid was applied dropwise to immobilize GOx and kept at 4 °C for 72 h. The target biosensor $TiO_2$NTs/Au/Pt/GOx was finally obtained.

## ■ ASSOCIATED CONTENT

### Supporting Information

The Supporting Information is available free of charge at https://pubs.acs.org/doi/10.1021/acsomega.1c06787.

Materials and reagents; characterization instruments; photoelectrochemical enzyme sensing experimental details, PEC test conditions and equipment; calculation formula of detection limit; SEM images of $TiO_2$NTs and $TiO_2$NTs/M (M = Au, Pt); *i*−*t* responses and linear calibration of PEC biosensors [$TiO_2$NTs and $TiO_2$NTs/M (M = Au, Pt)]; CV comparison of $TiO_2$NTs and $TiO_2$NTs/M (M = Au, Pt); TEM and HR-TEM images of $TiO_2$NTs and $TiO_2$NTs/M (M = Au, Pt); and photoelectric response *i*−*t* diagram of the electrode under different deposition conditions (PDF)

## ■ AUTHOR INFORMATION

### Corresponding Authors

**Delun Chen** − *State Key Laboratory of Marine Resource Utilization in South China Sea, College of Materials Science*



https://doi.org/10.1021/acsomega.1c06787
*ACS Omega* 2022, 7, 2474−2483

*and Engineering, Hainan University, Haikou 570228, China*; Email: chendelun2014@163.com

**Qiang Wu** − *Department of Clinical Laboratory of the Second Affiliated Hospital, School of Tropical Medicine and Laboratory Medicine, Key Laboratory of Emergency and Trauma of Ministry of Education, Research Unit of Island Emergency Medicine, Chinese Academy of Medical Sciences (No. 2019RU013), Hainan Medical University, Haikou 571199, China*; orcid.org/0000-0003-3922-5189; Email: wuqiang001001@aliyun.com

### Authors

**Zhuo Yang** − *State Key Laboratory of Marine Resource Utilization in South China Sea, College of Materials Science and Engineering, Hainan University, Haikou 570228, China*

**Wei Xu** − *State Key Laboratory of Marine Resource Utilization in South China Sea, College of Materials Science and Engineering, Hainan University, Haikou 570228, China*

**Bingdong Yan** − *State Key Laboratory of Marine Resource Utilization in South China Sea, College of Materials Science and Engineering, Hainan University, Haikou 570228, China*

**Baiqiang Wu** − *State Key Laboratory of Marine Resource Utilization in South China Sea, College of Materials Science and Engineering, Hainan University, Haikou 570228, China*

**Jinxin Ma** − *State Key Laboratory of Marine Resource Utilization in South China Sea, College of Materials Science and Engineering, Hainan University, Haikou 570228, China*

**Xiaohong Wang** − *State Key Laboratory of Marine Resource Utilization in South China Sea, College of Materials Science and Engineering, Hainan University, Haikou 570228, China*

**Bin Qiao** − *Department of Clinical Laboratory of the Second Affiliated Hospital, School of Tropical Medicine and Laboratory Medicine, Key Laboratory of Emergency and Trauma of Ministry of Education, Research Unit of Island Emergency Medicine, Chinese Academy of Medical Sciences (No. 2019RU013), Hainan Medical University, Haikou 571199, China*

**Jinchun Tu** − *State Key Laboratory of Marine Resource Utilization in South China Sea, College of Materials Science and Engineering, Hainan University, Haikou 570228, China*; orcid.org/0000-0001-8793-4727

**Hua Pei** − *Department of Clinical Laboratory of the Second Affiliated Hospital, School of Tropical Medicine and Laboratory Medicine, Key Laboratory of Emergency and Trauma of Ministry of Education, Research Unit of Island Emergency Medicine, Chinese Academy of Medical Sciences (No. 2019RU013), Hainan Medical University, Haikou 571199, China*

Complete contact information is available at: https://pubs.acs.org/10.1021/acsomega.1c06787

### Notes

The authors declare no competing financial interest.

## ■ ACKNOWLEDGMENTS

We gratefully acknowledge the project supported by the Finance Science and Technology Project of Hainan Province (nos. 2019RC114, 2019RC221, 820RC647, ZDKJ2021029, and ZDYF2021SHFZ068), Hainan Province Clinical Medical Center, the National Natural Science Foundation of China (nos. 51762012, 51862006, 81860373, 81902154, and 82060386), CAMS Innovation Fund for Medical Sciences (no. 2019-I2M-5-023), and the Key Laboratory Open Project Fund of Emergency and Trauma of Ministry of Education (no. KLET-202008).

## ■ REFERENCES

(1) Osterloh, F. E. Inorganic nanostructures for photoelectrochemical and photocatalytic water splitting. *Chem. Soc. Rev.* **2013**, *42*, 2294−2320.

(2) Zhang, K.; Lv, S.; Zhou, Q.; Tang, D. CoOOH nanosheets-coated g-C3N4/CuInS2 nanohybrids for photoelectrochemical biosensor of carcinoembryonic antigen coupling hybridization chain reaction with etching reaction. *Sens. Actuators, B* **2020**, *307*, 127631. Shu, J.; Tang, D. Recent Advances in Photoelectrochemical Sensing: From Engineered Photoactive Materials to Sensing Devices and Detection Modes. *Anal. Chem.* **2020**, *92*, 363−377. Lv, S.; Zhang, K.; Zhu, L.; Tang, D. ZIF-8-Assisted NaYF4:Yb,Tm@ZnO Converter with Exonuclease III-Powered DNA Walker for Near-Infrared Light Responsive Biosensor. *Anal. Chem.* **2020**, *92*, 1470−1476.

(3) Zhao, W.-W.; Xu, J.-J.; Chen, H.-Y. Photoelectrochemical enzymatic biosensors. *Biosens. Bioelectron.* **2017**, *92*, 294−304.

(4) Hou, T.; Zhang, L.; Sun, X.; Li, F. Biphasic photoelectrochemical sensing strategy based on in situ formation of CdS quantum dots for highly sensitive detection of acetylcholinesterase activity and inhibition. *Biosens. Bioelectron.* **2016**, *75*, 359−364.

(5) Chen, Y.; Li, X.; Cai, G.; Li, M.; Tang, D. In situ formation of (0 0 1)TiO2/Ti3C2 heterojunctions for enhanced photoelectrochemical detection of dopamine. *Electrochem. Commun.* **2021**, *125*, 106987.

(6) Cai, G.; Yu, Z.; Ren, R.; Tang, D. Exciton-Plasmon Interaction between AuNPs/Graphene Nanohybrids and CdS Quantum Dots/TiO2 for Photoelectrochemical Aptasensing of Prostate-Specific Antigen. *ACS Sens.* **2018**, *3*, 632−639.

(7) Shu, J.; Qiu, Z.; Lv, S.; Zhang, K.; Tang, D. Plasmonic Enhancement Coupling with Defect-Engineered TiO2-x: A Mode for Sensitive Photoelectrochemical Biosensing. *Anal. Chem.* **2018**, *90*, 2425−2429.

(8) Sun, J.; Zhang, M.; Wang, Z.-F.; Chen, H.-Y.; Chen, Y.; Murakami, N.; Ohno, T. Synthesis of anatase TiO2 with exposed {001} and {101} facets and photocatalytic activity. *Rare Met.* **2019**, *38*, 287−291.

(9) Hou, Y.; Li, X.; Zou, X.; Quan, X.; Chen, G. Photoeletrocatalytic Activity of a Cu2O-Loaded Self-Organized Highly Oriented TiO2 Nanotube Array Electrode for 4-Chlorophenol Degradation. *Environ Sci Technol* **2009**, *43*, 858−863. Tang, H.-L.; Ren, Y.; Wei, S.-H.; Liu, G.; Xu, X.-X. Preparation of 3D ordered mesoporous anatase TiO2 and their photocatalytic activity. *Rare Met.* **2019**, *38*, 453−458.

(10) Ye, M.; Gong, J.; Lai, Y.; Lin, C.; Lin, Z. High-Efficiency Photoelectrocatalytic Hydrogen Generation Enabled by Palladium Quantum Dots-Sensitized TiO2 Nanotube Arrays. *J. Am. Chem. Soc.* **2012**, *134*, 15720−15723.

(11) Hou, Y.; Li, X.; Zhao, Q.; Chen, G.; Raston, C. L. Role of Hydroxyl Radicals and Mechanism of Escherichia coli Inactivation on Ag/AgBr/TiO2 Nanotube Array Electrode under Visible Light Irradiation. *Environ. Sci. Technol.* **2012**, *46*, 4042−4050.

(12) Mor, G. K.; Shankar, K.; Paulose, M.; Varghese, O. K.; Grimes, C. A. High efficiency double heterojunction polymer photovoltaic cells using highly ordered TiO2 nanotube arrays. *Appl. Phys. Lett.* **2007**, *91*, 152111 (acccessed 2021/08/19).

(13) Shen, S.; Chen, J.; Wang, M.; Sheng, X.; Chen, X.; Feng, X.; Mao, S. S. Titanium dioxide nanostructures for photoelectrochemical applications. *Prog. Mater. Sci.* **2018**, *98*, 299−385.

(14) Melvin, A. A.; Illath, K.; Das, T.; Raja, T.; Bhattacharyya, S.; Gopinath, C. S. M-Au/TiO2(M = Ag, Pd, and Pt) nanophotocatalyst for overall solar water splitting: role of interfaces. *Nanoscale* **2015**, *7*, 13477−13488.

(15) Wu, L.; Li, F.; Xu, Y.; Zhang, J. W.; Zhang, D.; Li, G.; Li, H. Plasmon-induced photoelectrocatalytic activity of Au nanoparticles enhanced TiO2 nanotube arrays electrodes for environmental remediation. *Appl. Catal., B* **2015**, *164*, 217−224.

(16) Vaiano, V.; Iervolino, G.; Sannino, D.; Murcia, J. J.; Hidalgo, M. C.; Ciambelli, P.; Navío, J. A. Photocatalytic removal of patent blue V

dye on Au-TiO 2 and Pt-TiO 2 catalysts. *Appl. Catal., B* **2016**, *188*, 134−146.
(17) Zhai, D.; Liu, B.; Shi, Y.; Pan, L.; Wang, Y.; Li, W.; Zhang, R.; Yu, G. Highly Sensitive Glucose Sensor Based on Pt Nanoparticle/Polyaniline Hydrogel Heterostructures. *ACS Nano* **2013**, *7*, 3540−3546.
(18) Daniel, M.-C.; Astruc, D. Gold Nanoparticles: Assembly, Supramolecular Chemistry, Quantum-Size-Related Properties, and Applications toward Biology, Catalysis, and Nanotechnology. *Chem. Rev.* **2004**, *104*, 293−346.
(19) Tahir, M.; Tahir, B.; Amin, N. A. S. Synergistic effect in plasmonic Au/Ag alloy NPs co-coated TiO2 NWs toward visible-light enhanced CO2 photoreduction to fuels. *Appl. Catal., B* **2017**, *204*, 548−560.
(20) Seh, Z. W.; Liu, S.; Low, M.; Zhang, S.-Y.; Liu, Z.; Mlayah, A.; Han, M.-Y. Janus Au-TiO2Photocatalysts with Strong Localization of Plasmonic Near-Fields for Efficient Visible-Light Hydrogen Generation. *Adv. Mater.* **2012**, *24*, 2310−2314.
(21) Guo, N.; Zeng, Y.; Li, H.; Xu, X.; Yu, H. Crumpled and flexible cotton-fiber-like TiO2 with Pt anchored and its notable photocatalytic activity facilitate by Schottky junction interface. *Mater. Lett.* **2018**, *221*, 183−186.
(22) Macak, J. M.; Schmidt-Stein, F.; Schmuki, P. Efficient oxygen reduction on layers of ordered TiO2 nanotubes loaded with Au nanoparticles. *Electrochem. Commun.* **2007**, *9*, 1783−1787.
(23) Meekins, B. H.; Kamat, P. V. Got TiO2 Nanotubes? Lithium Ion Intercalation Can Boost Their Photoelectrochemical Performance. *ACS Nano* **2009**, *3*, 3437−3446.
(24) Wang, G.; Wang, Q.; Lu, W.; Li, J. Photoelectrochemical Study on Charge Transfer Properties of TiO2−B Nanowires with an Application as Humidity Sensors. *J. Phys. Chem. B* **2006**, *110*, 22029−22034.
(25) Ndamanisha, J. C.; Guo, L. Nonenzymatic glucose detection at ordered mesoporous carbon modified electrode. *Bioelectrochemistry* **2009**, *77*, 60−63.
(26) Çakıroğlu, B.; Özacar, M. A self-powered photoelectrochemical glucose biosensor based on supercapacitor Co3O4-CNT hybrid on TiO2. *Biosens. Bioelectron.* **2018**, *119*, 34−41.
(27) Selvarajan, S.; Alluri, N. R.; Chandrasekhar, A.; Kim, S.-J. BaTiO3 nanoparticles as biomaterial film for self-powered glucose sensor application. *Sens. Actuators, B* **2016**, *234*, 395−403.
(28) Wang, Y.; Liu, L.; Li, M.; Xu, S.; Gao, F. Multifunctional carbon nanotubes for direct electrochemistry of glucose oxidase and glucose bioassay. *Biosens. Bioelectron.* **2011**, *30*, 107−111.
(29) Yang, Z.; Tang, Y.; Li, J.; Zhang, Y.; Hu, X. Facile synthesis of tetragonal columnar-shaped TiO2 nanorods for the construction of sensitive electrochemical glucose biosensor. *Biosens. Bioelectron.* **2014**, *54*, 528−533.
(30) Wang, C.; Nie, X.-G.; Shi, Y.; Zhou, Y.; Xu, J.-J.; Xia, X.-H.; Chen, H.-Y. Direct Plasmon-Accelerated Electrochemical Reaction on Gold Nanoparticles. *ACS Nano* **2017**, *11*, 5897−5905. Wang, S. S.; Jiao, L.; Qian, Y.; Hu, W. C.; Xu, G. Y.; Wang, C.; Jiang, H. L. Boosting Electrocatalytic Hydrogen Evolution over Metal-Organic Frameworks by Plasmon-Induced Hot-Electron Injection. *Angew. Chem., Int. Ed.* **2019**, *58*, 10713−10717. Hu, W.-C.; Shi, Y.; Zhou, Y.; Wang, C.; Younis, M. R.; Pang, J.; Wang, C.; Xia, X.-H. Plasmonic hot charge carriers activated Ni centres of metal-organic frameworks for the oxygen evolution reaction. *J. Mater. Chem. A* **2019**, *7*, 10601−10609. Wang, S.-S.; Hu, W.-C.; Liu, F.-F.; Xu, Q.-Y.; Wang, C. Insights into direct plasmon-activated eletrocatalysis on gold nanostar via efficient photothermal effect and reduced activation energy. *Electrochim. Acta* **2019**, *301*, 359−365.


https://doi.org/10.1021/acsomega.1c06787
*ACS Omega* 2022, 7, 2474−2483